The Size and Shape of Molecular Ions and Their Relevance to the Packing of the Hexafluorophosphate Salts‡

Andrew L. Rohl and D. Michael P. Mingos *,†
Inorganic Chemistry Laboratory, University of Oxford, South Parks Road, Oxford OX1 3QR, UK

The volumes, surface areas, effective radii and shapes of inorganic ions have been used to rationalise the solid-state structures of a number of $[PF_6]^-$ salts. The effective radii of the cluster ions, derived from the volume contained within the van der Waals sphere of the atoms, may be used to calculate radius ratios for the salts which are used to interpret the observed solid-state structures. The distortions from the idealised inorganic salt structures have been related to the non-spherical nature of the ions, which have been calculated from their moments of inertia. A method for graphically displaying the shape of the ions using a thermal ellipsoid plotting program has been developed. Finally the lattice energies of the salts have been calculated using the atom–atom potential method and the results show that the charge interactions between polarised ions can produce a structure that deviates greatly from the close-packed ideal.

The packing of molecules in the solid state has a crucial effect on their properties.[1] The conductivity[2] and magnetic properties[3] of these salts and the non-linear optical properties of co-ordination[4] and organometallic[5] compounds depend on the packing properties of the molecules and ions in the crystal. Although the molecular design of solid-state materials which optimise these desirable physical properties will prove to be an increasingly important concern for inorganic chemists,[6] our understanding of packing effects remains at a very primitive stage of its development. There have been surprisingly few attempts to model the packing modes of inorganic and organometallic molecular compounds[7] and salts.[8,9]

In the first paper of this series, several molecular size and shapes descriptors were introduced. It was found that the best descriptor of size is the effective radii, which is calculated from the molecular volume, whilst the moments of inertia were shown to be good shape parameters. In this paper, these descriptors are used to rationalise the observed solid-state structures of some hexafluorophosphate salts. The Cambridge Structural Database[10] has revealed that there are over five hundred salts containing this anion and eleven of these were selected. These salts were chosen such that the ratio of anion to cation volumes varied over a substantial range, and the shapes of the cations provided examples of spherical, discoidal and cylindrical geometries. This analysis was limited to salts with a cation:anion ratio of unity and no solvent of crystallisation in the lattice.

The hexafluorophosphate salts were chosen because the anion has high symmetry, is spherical and of intermediate size (volume = 54 Å^3) between halides and tetraphenylborate (which will be discussed in the next paper in this series). Furthermore, the relative simplicity of the hexafluorophosphate anion minimises interpenetration of nearest neighbour cations into its van der Waals surface, in contrast to the tetraphenylborate anion which has large cavities in its surface.

† *Present address:* Department of Chemistry, Imperial College of Science, Technology and Medicine, South Kensington, London SW7 2AY, UK.

‡ *Supplementary data available* (No. SUP 56907, 4 pp.): centroid–centroid distances in the hexafluorophosphate salts and partial atomic charges of ions as calculated by extended Hückel theory. See Instructions for Authors, *J. Chem. Soc., Dalton Trans.*, 1992, Issue 1, pp. xx–xxv.

Calculation Methods

In the first paper[11] of this series the basic procedures for calculating the volumes (V_m), surface areas (S_m), moments of inertia (M_1, M_2, M_3) and effective radii (R_{eff}) of cations and anions were described in detail. The method used to calculate the volume is that of Gavezzotti.[12] The effective radius is defined from the volume by expression (1). The shape

$$R_{eff} = (3V_m/4\pi)^{\frac{1}{3}} \quad (1)$$

parameters are derived from the moments of inertia calculated without mass weighting.[13] If the largest moment is denoted M_1, the middle one M_2 and the smallest one M_3 then it is possible to define the following three indices [equations (2)–(4)]. The

$$F_s = M_3/M_1 \quad \text{spherical index} \quad (2)$$

$$F_c = 1 - [(M_2 + M_3)/2M_1] \quad \text{cylindrical index} \quad (3)$$

$$F_d = 1 - [2M_3/(M_1 + M_2)] \quad \text{discoidal index} \quad (4)$$

closer the values of the parameters are to unity, the closer the ion is to the geometry represented by the parameter.

The shapes of ions described by the moments of inertia can be best visualised by representing them as ellipsoids with axis lengths proportional to $3R_{eff}M_i/(M_1 + M_2 + M_3)$ (i = 1, 2 or 3).

The arrangement of anions about a cation or *vice versa* where either the anion or cation is non-spherical can then be seen by displaying these ellipsoids using a thermal ellipsoid plotting program.[14] The process of converting the directions of the moments in cartesian space into the directions of ellipsoids in unit-cell space is non-trivial. It was accomplished by reversing the well-known procedure in crystallography of transforming anisotropic thermal parameters from cell space to cartesian space.[15] First the ellipsoid lengths and directions are combined into a tensor in cartesian space (U_o) by equation (5),

$$U_o = V\Lambda V^T \quad (5)$$

where V is the 3 × 3 matrix of eigenvectors from the moments of inertia calculation and Λ is the 3 × 3 matrix with the ellipsoid lengths along the diagonal and zeros elsewhere. Note that the anisotropic thermal parameters in cell space are

expressed in Angstroms not in fractional units, so to convert the thermal parameters from cell- to cartesian-space, the usual cell to orthogonal transformation matrix (A) must have all references to the cell-edge lengths removed from it, *i.e.* it must consist of terms containing only the cell angles α, β, γ. This transformation matrix must also be post multiplied by a diagonal matrix D [whose elements are defined by equations (6) and (7)] since the ellipsoid matrix is a tensor. To achieve the

$$D_{11} = \sin\alpha/N,\ D_{22} = \sin\beta/N,\ D_{33} = \sin\gamma/N \quad (6)$$

$$N^2 = 1 + 2\cos\alpha\cos\beta\cos\gamma - \cos^2\alpha - \cos^2\beta - \cos^2\gamma \quad (7)$$

reverse of this process, the product of A and D must be inverted, yielding equation (8) for the tensor in cell space (U_c).

$$U_c = (AD)^{-1}U_o\{(AD)^{-1}\}^T \quad (8)$$

Ideal structural types are not commonly observed in molecular salts because of the presence of protrusions and indentations in the surface of molecular ions. These allow neighbouring ions to interlock and thus distortions from the ideal structural types often occur. This interlocking of ions has been termed *interpenetration*. A crude indicator of whether or not an ion is likely to interpenetrate with its surrounding ions is the R_{eff}/R_{max} ratio. A ratio near unity indicates that no interpenetration is possible, with increasing likelihood of interpenetration as the ratio decreases. Once the actual packing of a salt is known, three new quantities may be introduced which measure the degree of interpenetration present in the structure more precisely than the simple R_{eff}/R_{max} ratio. These three parameters are designated P_{c-a}, P_{c-c} and P_{a-a} and they describe the interpenetration between the cations and anions, the cations and cations, and the anions and anions respectively. These quantities are defined by equations (9)–(11), where R_{c-a},

$$P_{c-a} = R_{c-a} - (R_{eff}\text{cation} + R_{eff}\text{anion}) \quad (9)$$

$$P_{c-c} = R_{c-c} - 2R_{eff}\text{cation} \quad (10)$$

$$P_{a-a} = R_{a-a} - 2R_{eff}\text{anion} \quad (11)$$

R_{c-c} and R_{a-a} are the smallest cation–anion, cation–cation, and anion-anion centroid–centroid distances respectively. These parameters are thus simply the distances between cations and anions in the structure minus the distance expected if the ions are packed as rigid impenetrable spheres with radii corresponding to the effective radii of the ions. A negative result implies that some degree of interpenetration is occurring which will be substantial if its absolute value is greater than one.

The lattice energies E of the hexafluorophosphate salts were calculated using the pairwise atom–atom potential method based on expression (12) where r_{ij} is the non-bonded inter-

$$E = \sum_i \sum_j [Ae^{-Br_{ij}} - C/r_{ij}^6 + (q_iq_j/r_{ij})]/2 \quad (12)$$

molecular distance between atoms i and j, and q_i and q_j are the charges on the ith and jth atoms respectively. The index i is over all atoms in the asymmetric unit and j is over the surrounding ions. There is a similar sum within the asymmetric unit to account for interactions between the anion and cation within it. Terms A, B and C are adjustable constants that depend only on the specific atoms involved in the interaction and not on their valence state, molecular environment or other chemical characteristics. The potentials used for the non-metallic elements in this study are those of Williams and Houpt,[16] which were obtained from the fitting of the cell dimensions of many organic crystal structures. For the first-row transition metals the values used were those of Kr and for the second and third rows those of Xe[17] were utilised. This approximation has recently been used by Braga *et al.*[7] in calculating the packing energies of first-row transition-metal carbonyls.

The atomic charges were obtained from extended Hückel (EHT) calculations.[18] Although the charges from EHT calculations are not completely reliable, the size of these ions as well as the presence of transition metals and unpaired electrons makes these ions unsuitable for more rigorous techniques such as complete neglect of differential overlap (CNDO) or *ab initio* methods. Another justification for the use of the EHT method is that we are comparing results between systems with the same constituent ions and so it is the relative charges which are important not the absolute values. In this work the charges returned by the EHT program have been averaged over chemically equivalent atoms.

These lattice-energy calculations were carried out using the PCK83 program of Williams.[19] The charge term in the expression for the lattice energy converges very slowly since it is dependent on r^{-1} but PCK83 uses the Ewald summation which speeds up the convergence dramatically.

A computer program, which calculates the size and shape quantities discussed in this paper, is available. It is written in C and runs on Apple Macintosh Computers.

Results and Discussion

Table 1 summarises the important parameters for the $[PF_6]^-$ salts analysed in the present study. The volumes of the cations in these salts vary from 91 to 795 Å^3. The calculated ratios of anion to cation radii (a/c ratio) for the structures range from 0.84 to 0.41. For comparative purposes, the idealised minimum radius ratios for simple inorganic structures are listed in Table 2. These data suggest that on the basis of size effects alone, the hexafluorophosphate salt **1** in Table 1 should adopt an eight-co-ordinate structure and the salts **3**–**10** six-co-ordinate structures. Salt **2** lies on the boundary between six- and eight-co-ordination and so either packing mode is expected, whilst salt **11** is on the boundary between four- and six-co-ordination. The structure type of a salt is deduced from an examination of the co-ordination numbers (c.n.s) of the cations and anions in the salt. We have defined the co-ordination number of a cation as the number of anions that are closer than the nearest-neighbour cation to this cation. The co-ordination number of the anion is defined similarly.

The cations **1** and **7** listed in Table 1 are spherical-top ions, because their calculated moments of inertia are equal. The cations **2**, **6** and **11** have spherical indices (F_s) between 0.78 and 0.83, indicating that they are close to being spherical. Cations **4** and **5** are far from spherical and have significant discoidal components. Cation **9** has a distinct cylindrical component, whilst the remainder are asymmetric with cation **3** particularly so.

In the following section, the structures of these hexafluorophosphate salts are described in the context of the previously introduced size and shape parameters. The salts are presented in order of decreasing a/c ratio.

$[NMe_4][PF_6]$.—The a/c ratio of this salt is 0.84, suggesting that a CsCl type structure will be adopted in the solid state. Furthermore the deviations from an ideal CsCl structure are expected to be small since the cation is essentially spherical. This is indeed the case as illustrated by the sphere packing diagram in Fig. 1. The eight cations form an elongated cube with edge lengths of 5.97 and 6.09 Å around the anion. The anion is not centred in the elongated cube, being 2.51 Å from one square face and 3.58 Å from the other. The distorted cube of anions around the cation may be considered as two interpenetrating tetrahedra. In each tetrahedron, the distance from the anion to each of the cations is the same. Each tetrahedron can be characterised by its internal angles. The

Table 1 Size and shape parameters of the cations from the hexafluorophosphate salts studied

Salt	Cation	Space group	a/c	V_m/ Å^3	S_m/ Å^2	R_{eff}/ Å	R_{max}/ Å	R_{eff}/R_{max}	M_1/ Å^2	M_2/ Å^2	M_3/ Å^2	F_s	F_c	F_d	C_k (%)	Ref.
1	$[NMe_4]^+$	*P4/nmm*	0.84	91	123	2.79	3.27	0.85	21	21	21	1.00	0.00	0.00	66.9	20
2	$[Fe(\eta^5\text{-}C_5H_5)(CO)_3]^+$	*Pbca*	0.73	140	166	3.22	4.69	0.69	34	29	28	0.83	0.15	0.11	64.6	21
3	$[Ru(N_3)(N_2)(en)_2]^+$ [a]	$P2_1/n$	0.65	194	244	3.59	5.15	0.70	152	59	41	0.27	0.67	0.61	67.4	22
4	$[Fe(CO)_3(\eta^5\text{-}C_6Me_7)]^+$ [b]	$Pca2_1$	0.58	271	303	4.01	5.50	0.73	154	148	90	0.59	0.22	0.40	65.4	23
5	$[Fe(\eta^5\text{-}C_{11}H_{11})_2]^+$ [c]	$P\bar{1}$	0.56	302	339	4.16	5.88	0.71	210	178	116	0.55	0.30	0.40	68.6	24
6	$[Co(\eta^6\text{-}C_6Me_6)_2]^+$	*Pnnm*	0.53	361	397	4.42	5.50	0.80	268	264	216	0.81	0.10	0.19	68.9	25
7	$[Ni_6(\eta^5\text{-}C_5H_5)_6]^+$	*Pa3*	0.49	470	504	4.82	5.45	0.88	316	316	316	1.00	0.00	0.00	71.5	26
8	$[Ru(cod)(PMe_2Ph)_3]^+$ [d]	*Pbca*	0.46	537	565	5.04	8.02	0.63	690	461	316	0.46	0.44	0.45	70.2	27
9	$[Co(NO)_2(PPh_3)_2]^+$	*C2/c*	0.46	550	611	5.08	8.66	0.59	790	435	360	0.46	0.50	0.41	67.8	28
10	$[Mn(CO)_2\{P(OMe)_2Ph\}_4]^+$	*P2/c*	0.43	658	727	5.40	8.68	0.62	952	641	553	0.58	0.37	0.31	68.0	29
11	$[Au(PPh_2Me)_4]^+$	*P4/ncc*	0.41	795	879	5.75	8.28	0.69	1095	858	858	0.78	0.22	0.12	69.9	30
	$[PF_6]^-$			54	82	2.34	2.88	0.81	5	5	5	1.00	0.00	0.00		

[a] en = Ethane-1,2-diamine. [b] $C_6Me_7^-$ = Heptamethylcyclohexadienyl. [c] $C_{11}H_{11}^-$ = 1,3-Dimethylindenyl. [d] cod = Cycloocta-1,4-diene.

Table 2 The minimum radius ratios for a given co-ordination number

Co-ordination polyhedron	c.n.	Minimum radius ratio
Trigonal	3	0.155
Tetrahedral	4	0.255
Octahedral	6	0.414
Cubic	8	0.732
Cuboctahedral	12	1.000

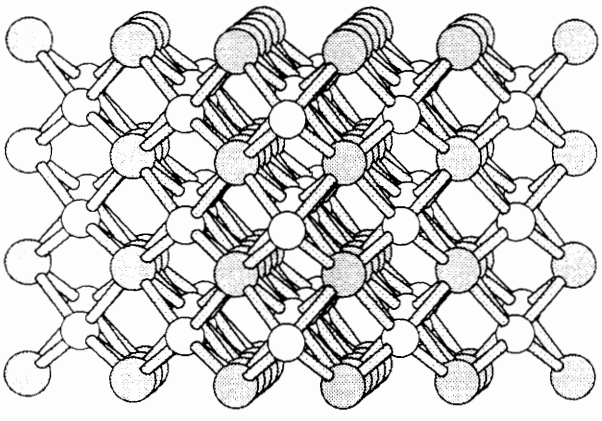

Fig. 1 The sphere representation of the packing in $[NMe_4][PF_6]$ viewed down the 0*ab* axis

tetrahedron consisting of the four closest anions has two angles of 99.3°, and all the other internal angles equal to 114.8°. The other tetrahedron has two angles of 118.5°, and all the other internal angles equal to 105.1°.

The deviations of the arrangement of anions around a cation from an ideal cube can be rationalised by considering the tetrahedral nature of the cation. The four closest anions surrounding a cation are centred at the *faces* of the $[NMe_4]^+$ tetrahedron, forming in turn another tetrahedron. The four farthest anions are at the *vertices* of the $[NMe_4]^+$ cation, thus forming a larger tetrahedron. The four closest cations about an anion are orientated such that a face of each $[NMe_4]^+$ tetrahedron points at a $[PF_6]^-$ face whilst the four farthest are orientated such that a vertex of each $[NMe_4]^+$ tetrahedron points at a $[PF_6]^-$ face. Note that the deviations from an idealised CsCl structure arise primarily from the shape of the cation, since it is larger than the anion. This is manifest in the solid state packing of $[NMe_4][ClO_4]$ [31] which is isostructural with $[NMe_4][PF_6]$. The anion in the former salt is tetrahedral but the arrangement of cations about the anion is the same in the two structures despite the differences in anion geometry.

$[Fe(\eta^5\text{-}C_5H_5)(CO)_3][PF_6]$.—The a/c ratio of this salt is 0.73 which lies on the boundary between six- and eight-co-ordination. The salt adopts a distorted *anti*-NiAs structure in the solid state, where the cations lie in a distorted trigonal prism of anions and the anions lie in a distorted octahedral environment of cations. These two different co-ordination polyhedra are visible in the sphere representation of the packing of $[Fe(\eta^5\text{-}C_5H_5)(CO)_3][PF_6]$, pictured in Fig. 2. The octahedra are tilted the same way horizontally but alternate their tilt vertically. Although the tilt of the octahedra is identical horizontally, neighbouring octahedra are rotated relative to each other by 180° about their long tilted axes, leading to the two anion sites visible in the figure.

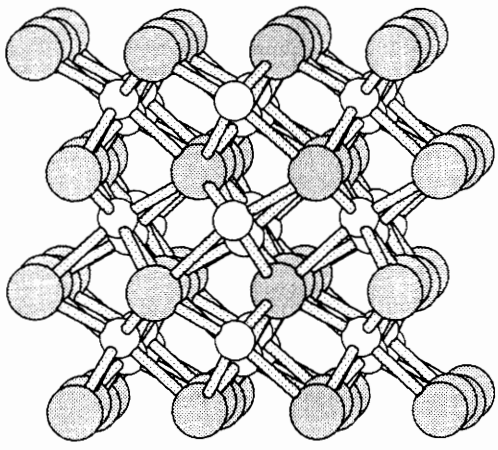

Fig. 2 The sphere representation of the packing in $[Fe(\eta^5\text{-}C_5H_5)(CO)_3][PF_6]$ viewed down the 0*a* axis

The shape factors indicate that the cation is nearly spherical with a slight cylindrical distortion. The distortion of the arrangement of anions around a cation from an ideal trigonal prism is rather small with an average triangular edge length of 7.56 Å and a maximum deviation of 0.68 Å. The distance between each atom in a triangular face and the one below it in the other triangle is constant at 6.21 Å. The anion is not equidistant between these two triangles; rather it is situated 2.73 Å from one and 3.39 Å from the other. If the first and sixth nearest-neighbour cations about an anion are taken to occupy apical positions, then the remaining four nearest-neighbour cations are arranged in an approximate square about the anion. They are not coplanar with the anion, with a maximum deviation of 0.50 Å from the best plane through them. The vectors formed between the two apical cations and the anion make angles of 85.9 and 84.7° with this best plane.

The arrangement of anions around a cation is given in Fig. 3. Three of the $[PF_6]^-$ ions form a triangle centred around the CO group which is immediately below the cyclopentadienyl ring.

The remaining three $[PF_6]^-$ ions form another triangle that is not *anti* to the first, thus forming a trigonal prism rather than an octahedron. The cation is not octahedrally co-ordinated because the cyclopentadienyl ring is too large to fit in a trigonal face. Instead the cation adopts a trigonal-prismatic co-ordination which has square faces large enough to accommodate the cyclopentadienyl ring.

$[Ru(N_3)(N_2)(en)_2][PF_6]$.—The *a*/*c* ratio of this salt is 0.65, suggesting that a six-co-ordinate structure will be adopted in the solid state. The observed co-ordination number of this salt is five. This five-co-ordinate structure consists of ions in very distorted trigonal-bipyramidal environments. The packing sequence of these trigonal bipyramids is complex, leading to them having many different orientations. The $[Ru(N_3)(N_2)(en)_2]^+$ cation is the most unsymmetrical of the eleven studied, with its geometry tending towards cylindrical. Examination of both the cation and anion environments failed to explain this observed solid-state structure. This suggests that something other than size and shape factors are determining the solid-state structure of this salt. A significant clue as to why this salt adopts such an unusual structure can be found in the packing diagram shown in Fig. 4. The hexafluorophosphate ions lie in pairs in cavities in the structure. The two anions making each pair are not at the same level, rather one is in a layer consisting of anions and cations with the other in a layer below the first. There are also cavities in the structure in which the azide groups accumulate. The N_2 groups on cations on adjacent layers stack almost on top of each other with N_3 groups from cations within the same layers lying nearby. Extended Hückel calculations, which will be discussed in full later, show that the residual charges on the azide groups are large and alternate in sign along the chain, thus making Coulombic interactions between these groups very favourable. This is probably the reason for this salt adopting such an unusual packing motif.

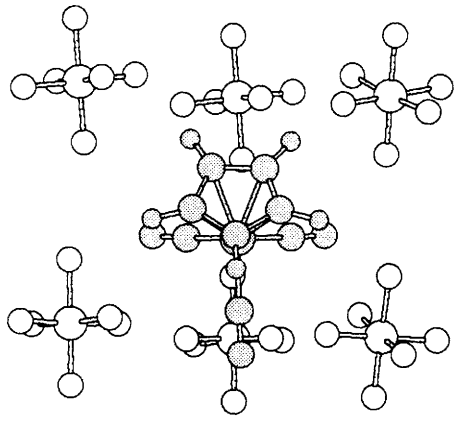

Fig. 3 The trigonal-prismatic arrangement of the six nearest-neighbour anions about a cation in $[Fe(\eta^5\text{-}C_5H_5)(CO)_3][PF_6]$

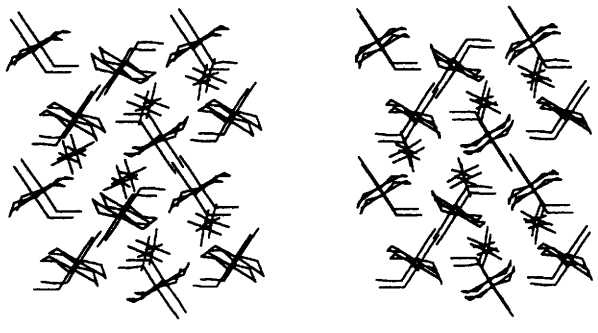

Fig. 4 A stereogram of the packing in $[Ru(N_3)(N_2)(en)_2][PF_6]$

$[Fe(CO)_3(\eta^5\text{-}C_6Me_7)][PF_6]$.—The *a*/*c* ratio for this salt is 0.58 which suggests a six-co-ordinate structural type. This salt adopts an *anti*-NiAs structure similar to the one found for $[Fe(\eta^5\text{-}C_5H_5)(CO)_3][PF_6]$. The shape factors of the cation indicate that it has a significant discoidal component to its shape. The influence of the shape of the cation on the spatial arrangement of the nearest neighbour anions can be clearly seen in Fig. 5(*a*). The trigonal-prismatic co-ordination of the cation is plainly visible, but it is noteworthy that two of the hexafluorophosphate anions lie in the plane of the two long axes of the discoidal cation and the remaining four lie near the short axis. This arrangement is reflected in the calculated cation–anion centroid distances, which show a distinct gap between the four nearest-neighbour distances and the fifth and sixth nearest neighbours. This distortion yields an average triangular edge length of 8.60 Å with a maximum deviation of 0.84 Å, which is appreciably larger than that observed in the more spherical $[Fe(\eta^5\text{-}C_5H_5)(CO)_3]^+$ system. The distance between each anion in a triangle and its neighbour below is 7.84 Å. The anion is not equidistant between these two triangles—it is 4.01 Å from one and 3.83 Å from the other.

The distorted octahedron of cations around an anion is depicted in Fig. 5(*b*). The four farthest nearest-neighbour cations are coplanar with the anion, forming an approximate square around it. The vectors formed between the two apical atoms and the anion make angles with this plane of 79.9° for the first nearest-neighbour cation and 78.4° for the second nearest-neighbour cation.

The arrangement of anions around a cation is given in Fig. 6. This arrangement is quite different from that found for $[Fe(\eta^5\text{-}C_5H_5)(CO)_3][PF_6]$. In this case it is impossible to fit three $[PF_6]^-$ anions around a CO group because of unfavourable interactions which would result between the larger ring and one

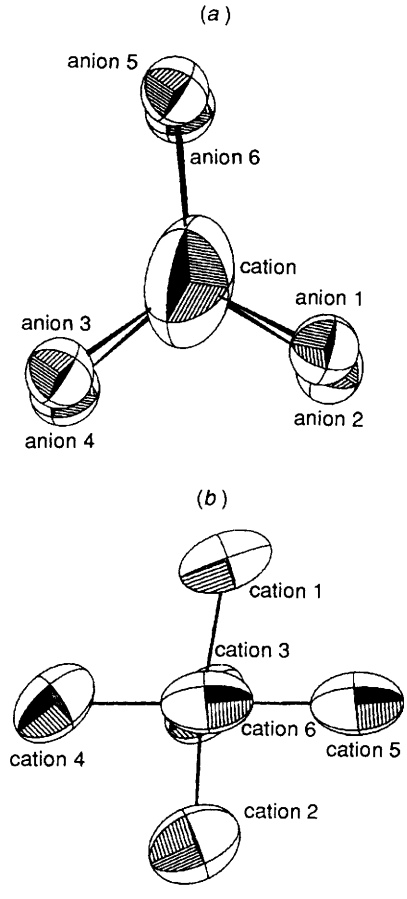

Fig. 5 Ellipsoid representations of (*a*) cation- and (*b*) anion-nearest neighbours in $[Fe(CO)_3(\eta^5\text{-}C_6Me_7)][PF_6]$. The larger the ion number the further it is from the central ion

of the $[PF_6]^-$ ions. Instead the three square faces of the trigonal prism accommodate the three CO groups, one side of the ring system, and the protruding methyl group respectively. The other side of the ring system is directed towards the two furthest hexafluorophosphate anions. It is noteworthy that a trigonal-prismatic co-ordination polyhedron has been adopted again, in which a large ring system has been incorporated into one of the large square faces.

$[Fe(\eta^5\text{-}C_{11}H_{11})_2][PF_6]$.—Although the nearest-neighbour distances for this salt indicate that the structure is five-co-ordinate, it is best described in terms of six-co-ordination. The sphere packing diagram of this salt, depicted in Fig. 7, shows that the structure can be thought of as a very distorted NaCl structure. The distortions take the form of translations between the horizontal four-co-ordinate layers. The cation has a distinct discoidal component to its shape, reflected in its large F_d value. The distorted octahedral arrangement of anions about a cation is shown in Fig. 8(*a*). The fifth and sixth nearest neighbours occupy the apical positions. The first four nearest-neighbour anions form a parallelogram around the cation, characterised by the edge lengths of 8.57 and 9.26 Å, and angles 91.3 and 88.7°. The vector from the cation to the fifth nearest-neighbour anion forms an angle of 69.9° with this plane, whilst the sixth nearest neighbour produces a corresponding angle of 56.4°. Note that the shape of the cation does not explain the large deviations of the two apical anions from their ideal positions. Furthermore, the orientation of the cation should lead to the sixth nearest-neighbour anion being closer than the fifth, since the sixth nearest-neighbour anion forms a smaller angle with the short axis of the cation.

In Fig. 8(*b*), the arrangement of nearest-neighbour cations around an anion is displayed. This arrangement is identical to that observed in Fig. 8(*a*), except that the fifth and sixth nearest neighbours are bent in the opposite direction. Note that the bending has brought the fifth and sixth cations in line with the first and second cations allowing them to pack tightly. The deviations of the four equatorial cations from a perfect square can also be rationalised from the figure—the discoidal shape of the cations prevents a perfectly square arrangement.

In Fig. 9, a section of the full packing diagram is illustrated. The four nearest-neighbour anions are placed in a plane around the central iron atom. This plane is not parallel to the two 1,3-dimethylindenyl rings and none of the anions interpenetrate into the cavity between these rings. The fifth and sixth anions lie above and below the two rings but very much to one side. The ideal apical sites are occupied by rings from a neighbouring cation, *i.e.* ring–ring interactions between different cations are responsible for the deviations from an ideal NaCl structure in this system. The intermolecular distance between rings is 3.41 (*cf.* 3.5 Å for twice the van der Waals radius of carbon). This implies that the surfaces of the two rings are in contact, as is shown in Fig. 10. The two 1,3-dimethylindenyl rings in contact are offset from each other such that the hydrogen atom on one six-membered ring lies above the centre of the other six-membered ring. Clearly there is a great deal of interaction between 1,3-dimethylindenyl rings on neighbouring cations. As a result, this salt may possess unusual magnetic and conductivity properties. Furthermore the protons which lie above the six-membered rings should give rise to unusual solid-state proton NMR signals.

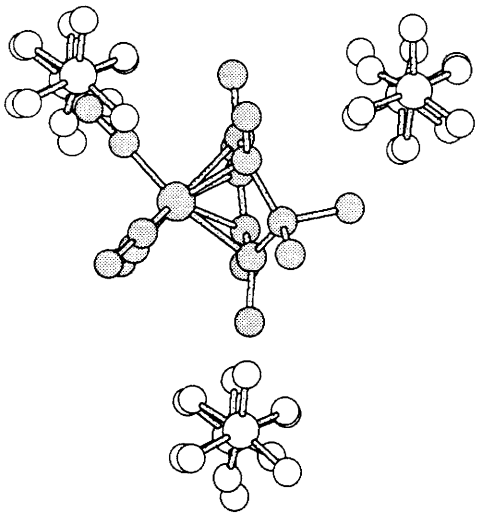

Fig. 6 The trigonal-prismatic arrangement of the six nearest-neighbour anions about a cation in $[Fe(CO)_3(\eta^5\text{-}C_6Me_7)][PF_6]$

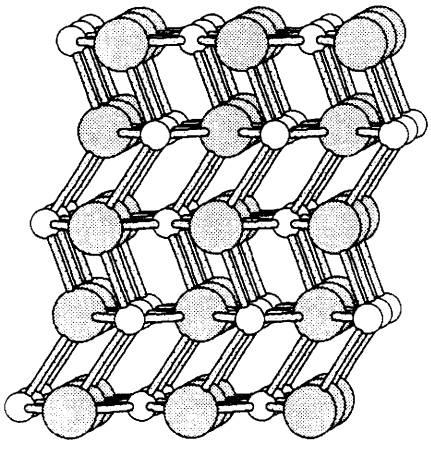

Fig. 7 The sphere representation of the packing in $[Fe(\eta^5\text{-}C_{11}H_{11})_2][PF_6]$ viewed down the 0*a* axis

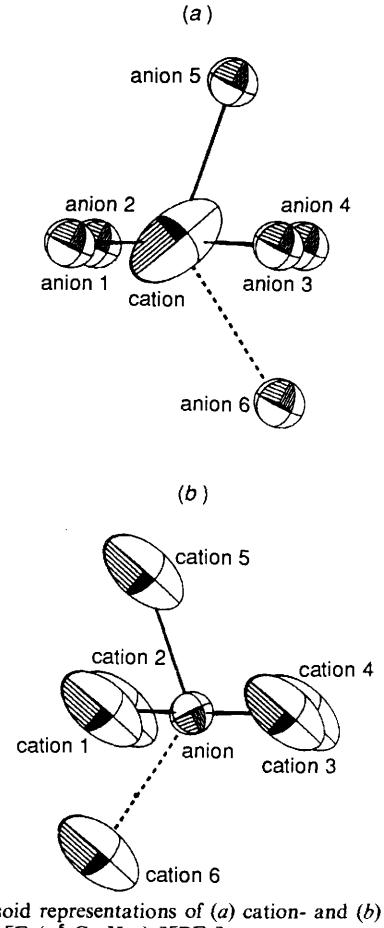

Fig. 8 Ellipsoid representations of (*a*) cation- and (*b*) anion-nearest neighbours in $[Fe(\eta^5\text{-}C_{11}H_{11})_2][PF_6]$

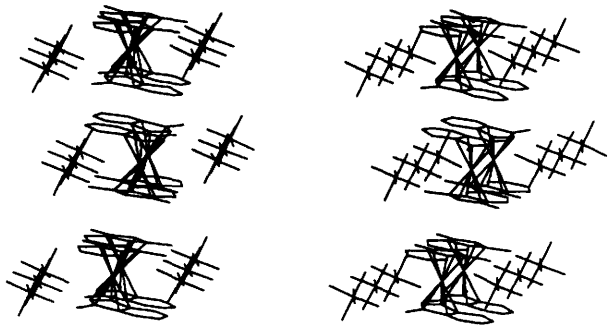

Fig. 9 A stereogram of the packing in $[Fe(\eta^5\text{-}C_{11}H_{11})_2][PF_6]$ showing the stacking of the cations

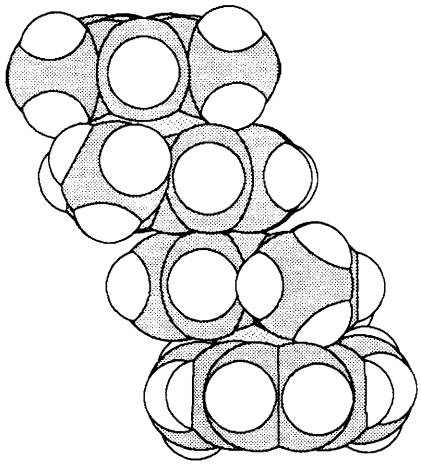

Fig. 10 Van der Waals representation of two neighbouring cations showing that the 1,3-dimethylindenyl rings are in contact

$[Co(\eta^6\text{-}C_6Me_6)_2][PF_6]$.—This salt adopts a distorted NaCl structure with two major distortions from an ideal NaCl structure. First the vertical ion–ion distances are longer than the horizontal ion–ion distances. Secondly the horizontal layers are formed by rectangles not squares. The cation is quite spherical with a slight discoidal distortion which is revealed in the ellipsoid representation of a cation's nearest-neighbour anions reproduced in Fig. 11(*a*). The co-ordination polyhedron is a distorted octahedron with the fifth and sixth nearest-neighbour anions occupying apical positions, *i.e.* the octahedron is elongated. The four equatorial cations are not arranged in a square around the cation but rather a rectangle with internal angles of 105.7 and 74.3°. The apical anions are both perpendicular to this rectangle and approach the cation directly along its principal axis thus they are slightly further away from the cation than the other four. The co-ordination polyhedron of the anion is identical and the view down the long axis of the octahedron is shown in Fig. 11(*b*). Note that the relative orientations of the equatorial cations imply that a rectangular arrangement will be more efficiently packed than a square arrangement since the short axes of the cations lie in the equatorial plane. The figure also illustrates that the orientations of cations vary between layers such that the long axes in one layer are nearly parallel to the short axes in the layer below, allowing closer packing between cation layers.

A view of the packing in this salt is given in Fig. 12. This figure shows that four of the anions are placed around the gap between the two rings as might be expected. These four anions consist of two equatorial and two axial anions. The other two equatorial anions sit above the rings but not at 90° to them. They are actually at a glancing angle of 15.7° from the perpendicular which places them above two methyl groups rather than the centre of the ring. The arrangement of the nearest-neighbour cations around an anion is also visible in

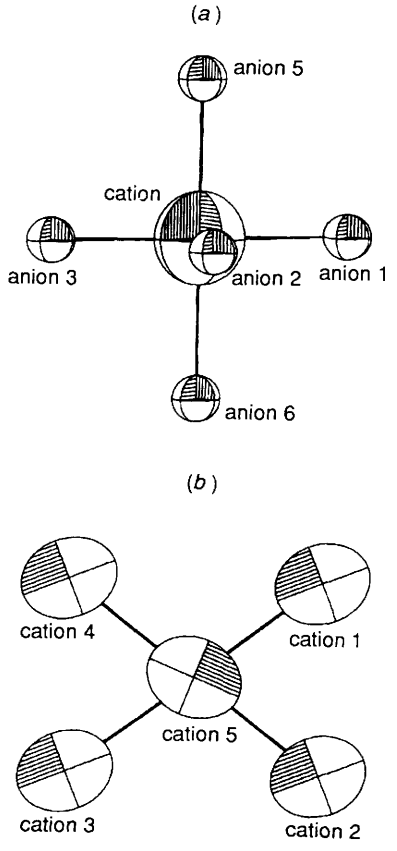

Fig. 11 Ellipsoid representations of (*a*) cation- and (*b*) anion-nearest neighbours in $[Co(\eta^6\text{-}C_6Me_6)_2][PF_6]$

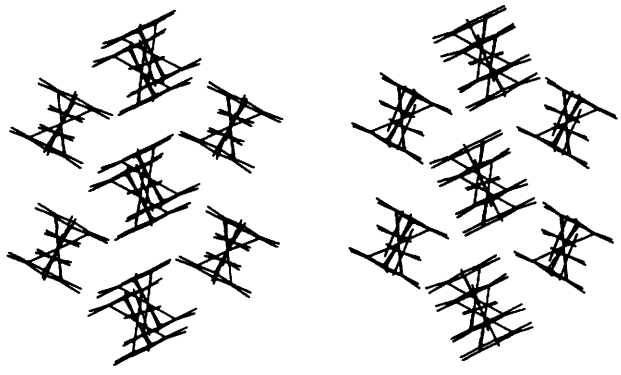

Fig. 12 A stereogram of the packing in $[Co(\eta^6\text{-}C_6Me_6)_2][PF_6]$ viewed down an approximate four-fold axis of the anion and cation octahedra

Fig. 12. Note that the distortion from the ideal square geometry to a rectangle has allowed overlap between methyl groups on methylbenzene rings with the methylbenzene group on neighbouring cations, *i.e.* ring–ring overlaps are responsible for distorting the geometry away from ideal. The two apical cations are orientated in such a way that each end of each of the two rings are in close proximity to the ends of rings on the equatorial cations.

$[Ni_6(\eta^5\text{-}C_5H_5)_6][PF_6]$.—This salt adopts a perfect NaCl structure in the solid state which is consistent with its a/c ratio of 0.49. This cation is the most spherical of all those studied in this paper, which is reflected in the absence of any deviations from an ideal NaCl structure. The nearest-neighbour anions about a cation are above six of the eight faces of its octahedron. They are not directly above the centres, rather they are shifted from the centre to form an octahedron. This is to be expected

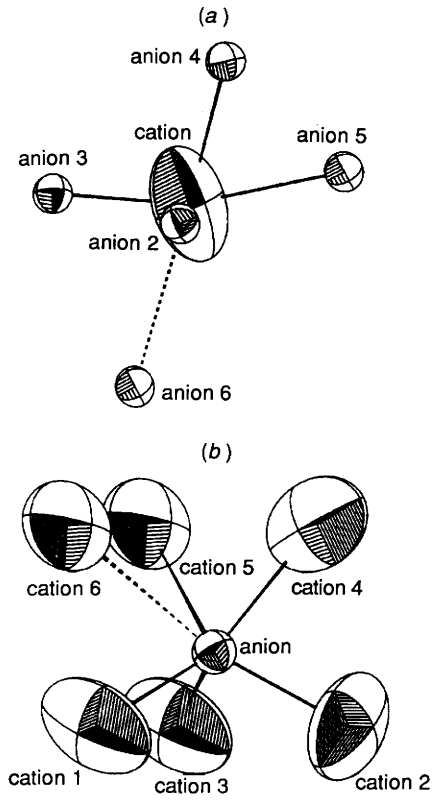

Fig. 13 Ellipsoid representations of (*a*) cation- and (*b*) anion-nearest neighbours in $[Ru(cod)(PMe_2Ph)_3][PF_6]$

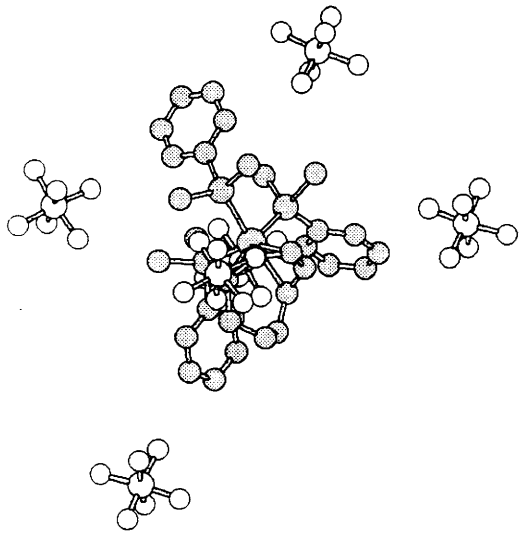

Fig. 14 The octahedron arrangement of the six nearest-neighbour anions about a cation in $[Ru(cod)(PMe_2Ph)_3][PF_6]$

since the edges and vertices of the nickel octahedron are inaccessible due to the presence of cyclopentadienyl rings. The arrangement of cations about an anion shows no obvious interactions between cations, further strengthening the premise that this cation is effectively spherical.

$[Ru(cod)(PMe_2Ph)_3][PF_6]$.—The nearest-neighbour distances for this salt indicate that its packing is based on five-co-ordination. However, the packing in this salt is best described by including the sixth nearest-neighbour anions and cations, producing a very distorted NiAs structure. The cation nearest neighbours, which are depicted in Fig. 13(*a*), are arranged

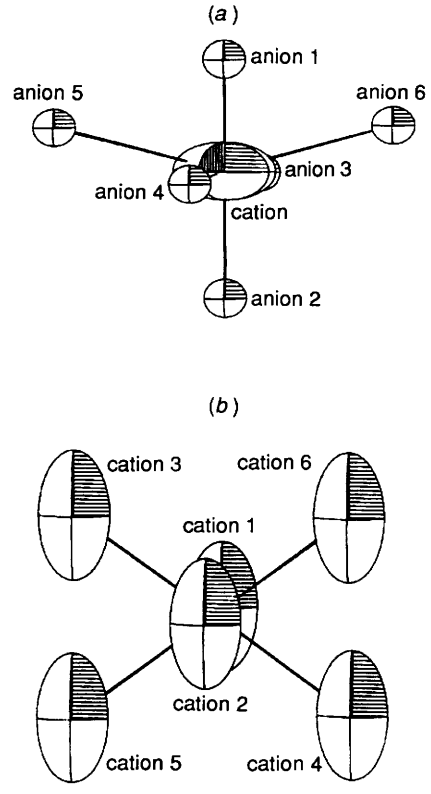

Fig. 15 Ellipsoid representations of (*a*) cation- and (*b*) anion-nearest neighbours in $[Co(NO)_2(PPh_3)_2][PF_6]$

about the cation to form a very distorted octahedron. The four equatorial ions are the first, second, third and fifth nearest-neighbour anions which are not coplanar, with a maximum deviation of 1.14 Å from the plane of best fit. Vectors from the fourth and six nearest neighbours to the cation produce angles of 64.7 and 65.5° respectively with this plane. The anion environment can also be more simply visualised if the sixth nearest-neighbour cation is included in the description. The resulting polyhedron, a distorted trigonal prism, is shown in Fig. 13(*b*). One triangular face consists of the first three nearest neighbours, the other by the fourth, fifth and sixth. The anion is 3.40 Å from the bottom triangular face and 5.90 Å from the other. These two triangles are greatly distorted from the ideal geometry and are very similar—the face closest to the anion has edges of lengths 11.96, 10.21 and 8.90 Å with angles of 56.4, 46.5 and 77.1°, whereas the other face has edge lengths of 11.96, 10.21 and 9.39 Å with angles of 55.6, 49.3 and 75.1°. These two triangular faces are not parallel.

The cation environment is reproduced in Fig. 14. The two closest anions are situated opposite each other, with the closest in between two PMe_2Ph units. The other sits over the cycloocta-1,4-diene ring. The other four are arranged around the bulky PMe_2Ph groups and so are further away. The approach of three of these to the cation is limited by the methyl groups. The fourth one, which is behind the cation, is in contact with a phenyl ring orientated end on, producing a sixth nearest-neighbour anion which is much further away from the cation than the other five.

$[Co(NO)_2(PPh_3)_2][PF_6]$.—The *a*/*c* ratio of 0.46 for this salt suggests a six-co-ordinate structure in the solid state. The actual structure adopted is a distorted NaCl structure in which the horizontal layers are not planar. The shape indices for the cation indicate that it is cylindrical. This is verified in the view of the cation's nearest-neighbour anions shown in Fig. 15(*a*). Two of the anions are much closer to the cation than the other four. These two anions occupy the apical positions in the

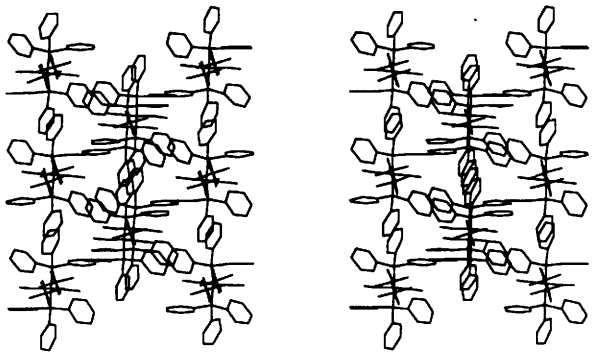

Fig. 16 A stereogram of the packing in $[Co(NO)_2(PPh_3)_2][PF_6]$ viewed down an approximate four-fold axis of the anion and cation octahedra

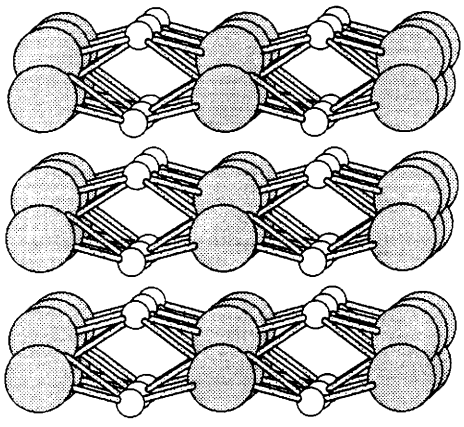

Fig. 17 The sphere representation of the packing in $[Mn(CO)_2\{P(OMe)_2Ph\}_4][PF_6]$ viewed down the 0*c* axis

distorted octahedron and lie immediately above and below one of the two short axes of the cation. Four additional anions lie part way between the other short axis and the long axis and are thus further away. These four anions are far from coplanar, with the two furthest being bent upwards by 15.2° out of the equatorial plane, whilst the other two neighbours are bent slightly down out of the equatorial plane. The two sets of opposing anions are not at right angles to each other, leading to anion–cation–anion angles of 72.2 and 109.1°. Again in this salt, the reasons for the deviations away from the ideal co-ordination polyhedron are not evident in the arrangement of anions about a cation.

The distorted octahedral arrangement of cations around an anion is shown in Fig. 15(*b*). This arrangement differs from that in Fig. 15(*a*) in that the two furthest neighbours are bent downwards out of the equatorial plane rather than upwards. The cations are all oriented with their long axes parallel [*cf.* Fig. 11(*b*)]. This arrangement explains why the four furthest cations are not coplanar—their principal axes are too long to pack in a plane.

A section of the packing in this salt is shown in Fig. 16. It shows that each cation has an anion located between the NO groups and another in the cavity between four phenyl groups. These two anions are the closest to each cation and the reason why they have unique centroid–centroid distances whilst the rest occur in pairs is clear. The two closest anions lie on the symmetry axis and therefore have independent local environments. The closest two of the four remaining anions are sitting in holes between two phenyl rings, leaving the furthest two at right angles to this each above a phenyl ring which is pointing directly at them. This clearly is not the most stable position for these two anions around an isolated cation. Fig. 15 suggests that the packing requirements of the cations with each other are overriding the energetically most stable arrangement of the

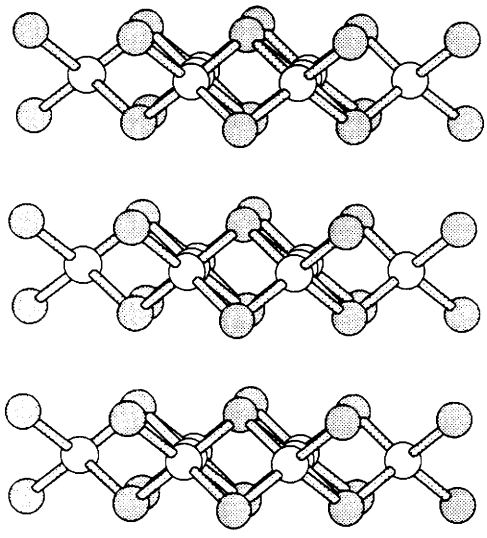

Fig. 18 The packing in PbO viewed down the *ab* axis

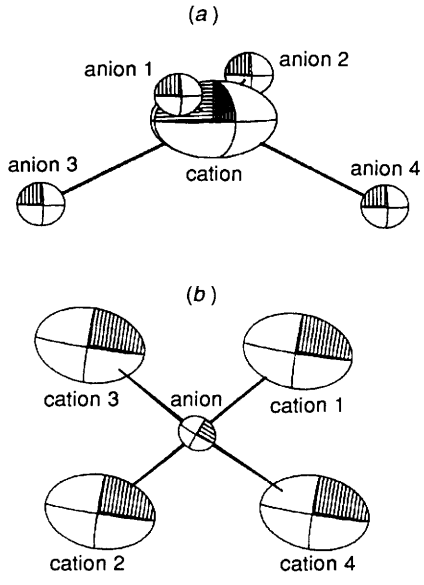

Fig. 19 Ellipsoid representation of (*a*) cation- and (*b*) anion-nearest neighbours in $[Mn(CO)_2\{P(OMe)_2Ph\}_4][PF_6]$

anions. The most striking feature is the interlocking of phenyl rings on neighbouring cations which produces the non-planar configuration of the equatorial ions of the co-ordination octahedra. The interacting phenyl rings are more than 4.5 Å away from each other, ruling out any cation–cation interactions leading to novel solid-state properties.

$[Mn(CO)_2\{P(OMe)_2Ph\}_4][PF_6]$.—This salt has an *a*/*c* ratio of 0.43, suggesting that a six-co-ordinate structure will be adopted in the solid state. In fact it forms a layer structure with the ions four-co-ordinated within the layers, as shown in Fig. 17. The cations have a distorted tetrahedral geometry and the anions a distorted square-planar structure, leading to layers which deviate greatly from planarity. This structure is very similar to the observed solid-state structures of LiOH and the red form of PbO.[32] The packing in the latter salt is reproduced in Fig. 18,[33] and shows the similarity between the two structures. In PbO, this structure is thought to be adopted because of the presence of lone pairs on the cation—the *a*/*c* ratio of this salt predicts a CsCl structure.

The arrangement of the four nearest-neighbour anions around a cation is depicted in Fig. 19(*a*). The cation is cylindrical in shape and the anions are arranged about the

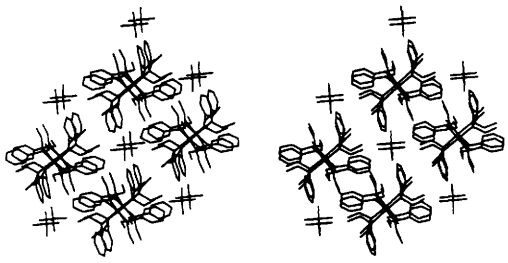

Fig. 20 A stereogram of the packing in $[Mn(CO)_2\{P(OMe)_2Ph\}_4][PF_6]$ viewed perpendicular to the four-co-ordinate layers

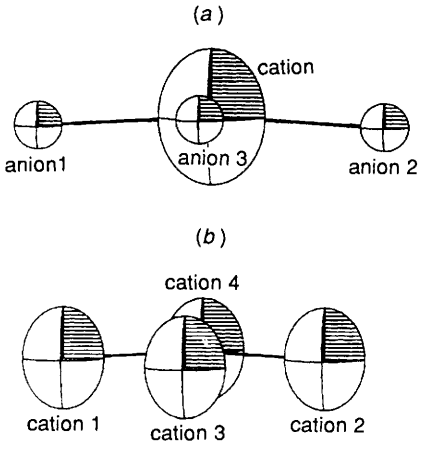

Fig. 21 Ellipsoid representations of (*a*) cation- and (*b*) anion-nearest neighbours in $[Au(PPh_2Me)_4][PF_6]$

plane through the large axis and one of the short axes. The anions are not coplanar, but they are a long way from being tetrahedral, the geometry which minimises anion–anion repulsion. The two furthest anions are bent down out of the equatorial plane by 26.9°, whilst the two closest are bent up by 12.8°. The two sets of anions are not at right angles to each other, leading to anion–cation–anion angles of 83.2 and 108.6°. Note that the two furthest anions approach the cation very close to its principal axis. The arrangement of the nearest-neighbour cations around an anion viewed perpendicular to the equatorial plane is shown in Fig. 19(*b*). The configuration is similar to Fig. 19(*a*), but both sets of cations are distorted up from the equatorial plane leading to cation–anion–cation angles of 71.5 and 96.8°. Note that the orientation of the cations with their principal axis almost aligned prevents the structure from adopting a planar configuration, similarly to the case for $[Co(NO)_2(PPh_3)_2][PF_6]$.

Fig. 20 shows a fragment of the packing in this salt. The two nearest anions to each cation are situated on opposite sides of the cation, sitting in a cavity produced between two OMe groups on one $P(OMe)_2Ph$ group and a OMe and Ph group on another. The other two ions are located on top of the surface produced by an OMe and Ph group on the same $P(OMe)_2Ph$ group. Again the positions of the anions are not that which would be taken if they were allowed to interact with an isolated cation. There are large cation–cation interactions occurring in this salt. These interactions take the form of a $P(OMe)_2Ph$ group on each cation slotting together and occur because each group is related by an inversion centre. This interaction occurs along the *trans* axis of each cation. There are also interactions occurring between neighbouring cations related by a translation which are quite different, because the *cis* $P(OMe)_2Ph$ groups do not approach each other head on, rather one group points up and the other is down and so these ions can come closer than those along the *trans* direction. Cation–cation interactions also appear to control this structure of this salt.

$[Au(PPh_2Me)_4][PF_6]$.—The *a*/*c* ratio of this salt is 0.41,

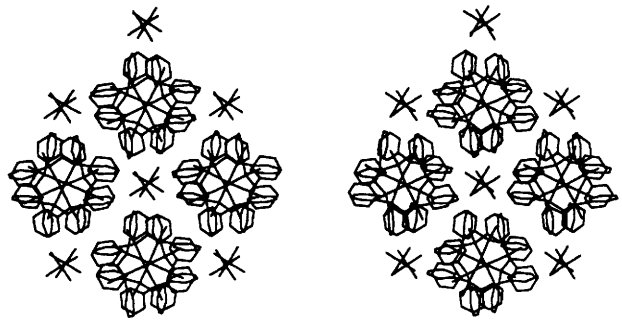

Fig. 22 A stereogram of the packing in $[Au(PPh_2Me)_4][PF_6]$ viewed perpendicular to the four-co-ordinate layers

which is very close to the boundary between four- and six-co-ordination. This salt adopts a four-co-ordinated structure which is based on square-planar co-ordination similarly to $[Mn(CO)_2\{P(OMe)_2Ph\}_4][PF_6]$, rather than the tetrahedral co-ordination found for the ZnS structures. This structure is also similar to the packing found in PbO and LiOH but has layers which are much closer to being planar. There is no known simple salt in which almost coplanar AX four-connected layers occur.[32]

The cation shape indices show that the cation has a cylindrical component to its shape. The arrangement of four anions around the cation is illustrated in Fig. 21(*a*). The anions are not quite coplanar, with two opposing anions lying above the cation and the other two below. The deviation is small leading to anion–cation–anion angles of 90.2 rather than 90°. The arrangement of cations about an anion is shown in Fig. 21(*b*). It is very similar to the cation's environment but this time all the anions lie above the cation resulting in cation–anion–cation angles of 89.9°. Note that the cations are all orientated with their primary axes vertical, which leads to a large interlayer distance since cations are stacked on top of cations.

A packing diagram of this salt is shown in Fig. 22. The anions and cations are not coplanar because of steric hindrance of a fluoride atom by the nearly vertical phenyl rings prevents the anion from sitting in a central position and so it is situated towards the flatter phenyl rings at the other end of the cation. The anions all lie around the middle of the cation, interpenetrating slightly between the phenyl rings. The environment about each anion is identical but inverted. This is a property of the cation and explains why the anions alternate between pointing up and down around the cation. The arrangement of the four cations about an anion viewed perpendicular to the equatorial plane is also shown in the figure. The four equatorial fluoride atoms on the anion appear to be pointing between two phenyl rings on each cation. Considering each cation as a square, it is interesting to note their arrangement. They are positioned such that they form a cavity which is just the right size to accommodate the $[PF_6]^-$ anion. Providing a cavity suitable for the anion must be an important part of the crystallisation process. Again it is cation–cation interactions which are causing this salt to adopt structures which deviate significantly from the idealised simple salt structure predicted from the *a*/*c* ratio.

Lattice Energy Calculations.—The lattice energies of the eleven hexafluorophosphate salts were calculated using two different approaches to the charge term. In the first method, a positive unit charge was placed at the centre of the cation and a negative unit charge was placed on the phosphorus atom of the anion. Secondly, partial atomic charges were generated from extended Hückel calculations and the atomic charges generated have been deposited (SUP 56907). The results are summarised in Table 3. There is a tendency for the van der Waals energy to become more negative as the cation increases in size. The inverse of this relationship holds for the Coulombic energy,

Table 3 Contributions towards the lattice energy of the hexafluorophosphate salts. E_v is the van der Waals energy, E_m^u is the Coulombic energy calculated using unit charges and E_m^p is the Coulombic energy calculated using partial atomic charges; ΔE is the change in lattice energy going from the unit-charge calculation to the partial atomic charge calculation. A negative value of ΔE indicates that stabilisation of the lattice has occurred using partial atomic charges

	E_v	E_m^u	E_m^p	
Salt	kJ mol^{-1}			ΔE(%)
$[NMe_4][PF_6]$	−48	−476	−436	8.3
$[Fe(\eta^5\text{-}C_5H_5)(CO)_3][PF_6]$	−93	−458	−528	−11.4
$[Ru(N_3)(N_2)(en)_2][PF_6]$	−65	−389	−568	−28.2
$[Fe(CO)_3(\eta^5\text{-}C_6Me_7)][PF_6]$	−76	−386	−454	−12.8
$[Fe(\eta^5\text{-}C_{11}H_{11})_2][PF_6]$	−142	−365	−353	2.4
$[Co(\eta^6\text{-}C_6Me_6)_2][PF_6]$	−150	−352	−345	1.5
$[Ni_6(\eta^5\text{-}C_5H_5)_6][PF_6]$	−197	−338	−368	−5.2
$[Ru(cod)(PMe_2Ph)_3][PF_6]$	−189	−320	−345	−4.8
$[Co(NO)_2(PPh_3)_2][PF_6]$	−211	−343	−356	−2.3
$[Mn(CO)_2\{P(OMe)_2Ph\}_4][PF_6]$	−186	−271	−411	−23.5
$[Au(PPh_2Me)_4][PF_6]$	−271	−301	−328	−4.6

Table 4 Summary of the packing modes of the hexafluorophosphate salts studied

Cation	a/c	c.n.	Structure type	F_s	F_c	F_d	P_{c-a}/Å	P_{c-c}/Å	P_{a-a}/Å
$[NMe_4]^+$	0.84	8:8	CsCl	1.00	0.00	0.00	−0.2	0.4	1.4
$[Fe(\eta^5\text{-}C_5H_5)(CO)_3]^+$	0.73	6:6	*anti*-NiAs	0.83	0.15	0.11	−0.6	0.6	1.5
$[Ru(N_3)(N_2)(en)_2]^+$	0.65	5:5	Five-co-ordinate	0.27	0.67	0.61	−0.8	−0.5	1.8
$[Fe(CO)_3(\eta^5\text{-}C_6Me_7)]^+$	0.58	6:6	*anti*-NiAs	0.59	0.22	0.40	−0.3	0.2	3.2
$[Fe(\eta^5\text{-}C_{11}H_{11})_2]^+$	0.56	5:5	NaCl	0.55	0.30	0.40	−0.6	−0.8	2.8
$[Co(\eta^6\text{-}C_6Me_6)_2]^+$	0.53	6:6	NaCl	0.81	0.10	0.19	0.0	−0.7	3.5
$[Ni_6(\eta^5\text{-}C_5H_5)_6]^+$	0.49	6:6	NaCl	1.00	0.00	0.00	0.0	0.5	5.4
$[Ru(cod)(PMe_2Ph)_3]^+$	0.46	5:5	NiAs	0.46	0.44	0.45	−0.6	−1.2	3.8
$[Co(NO)_2(PPh_3)_2]^+$	0.46	6:6	NaCl	0.46	0.50	0.41	−1.6	−0.4	4.7
$[Mn(CO)_2\{P(OMe)_2Ph\}_4]^+$	0.43	4:4	PbO Layer	0.58	0.37	0.31	−0.3	−1.4	4.7
$[Au(PPh_2Me)_4]^+$	0.41	4:4	PbO Layer	0.78	0.22	0.12	−0.7	−1.0	5.8

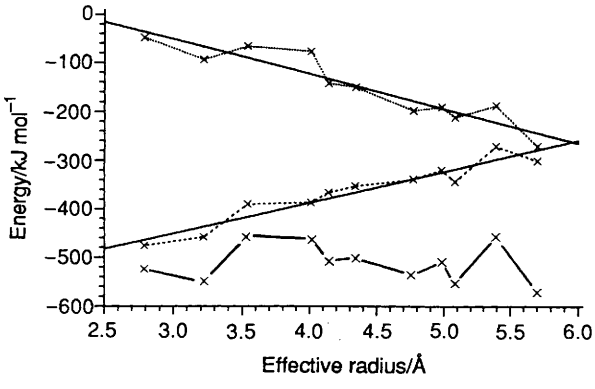

Fig. 23 A plot of unit-charge Coulombic (– – – –), van der Waals (· · · ·) and total energies (——) *versus* effective radius

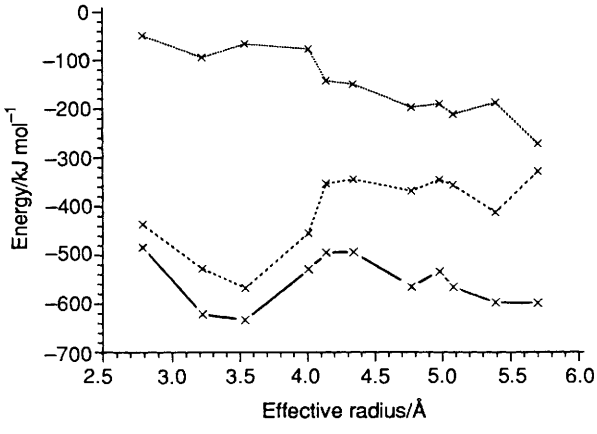

Fig. 24 A plot of partial-charge Coulombic (– – – –), van der Waals (· · · ·) and total energies (——) *versus* effective radius

irrespective of the model used. These trends can be seen in Fig. 23, where the unit-charge Coulombic, van der Waals and total (lattice) energies are plotted against the effective radius.

The van der Waals energy correlates approximately linearly with the effective radius with a correlation coefficient of 0.93; a result similar to that found for hydrocarbons by Gavezzotti.[34] The Coulombic energy calculated using unit charges of opposite sign centred on the anions and cations also correlates well with the effective radius, producing a correlation coefficient of 0.95. The overall effect of these two competing energies is to produce a fairly constant lattice energy of −510 kJ mol^{-1} with a standard deviation of 40 kJ mol^{-1}.

Note that of the three salts that have van der Waals energies above the line of best fit, two also have their Coulombic energies a long way above the Coulombic line of best fit. This means that those salts which have higher van der Waals energies than that predicted from their size generally do not have compensating Coulombic energies when calculated from unit charges.

In Fig. 24, a similar plot to Fig. 23 is drawn but with the Coulombic energy calculated using partial atomic charges. It is noteworthy that the Coulombic energy correlates much less well with the effective radius, leading to a correlation coefficient of 0.67. The three salts which have their van der Waals energy above the line of best fit have had a dramatic decrease in their Coulombic energies. This is a significant result since it implies that some salts are packed less densely than is possible, but these loosely packed configurations are stabilised by Coulombic interactions. In fact, these three salts ($[Ru(N_3)(N_2)(en)_2][PF_6]$, $[Fe(CO)_3(\eta^5\text{-}C_6Me_7)][PF_6]$, $[Mn(CO)_2\{P(OMe)_2Ph\}_4][PF_6]$) are amongst the six hexafluorophosphate salts with the lowest packing coefficients. This

suggests that partial atomic charges must be used in any calculations that attempt to model molecular salts; unit charges centred on the ions will not suffice. The only disturbing feature of the figure is the large oscillations in total lattice energies, but this is probably just an artefact of the charges generated by the extended Hückel method since it produces larger charge separations than those found by more rigorous and reliable methods. Methods that produce smaller polarisations would make the Coulombic energy more linearly dependent on the effective radius which in turn would make the lattice energy more constant.

Conclusions

The results for the hexafluorophosphate salts are summarised in Table 4. This table clearly shows a reduction in co-ordination number as the a/c ratio decreases. Ignoring the five-co-ordinate structures then leads to the series: $a/c \geqslant 0.84 \Rightarrow$ eight-co-ordination, $0.46 \leqslant a/c < 0.84 \Rightarrow$ six-co-ordination, $a/c < 0.46 \Rightarrow$ four-co-ordination. The most regular structural type is observed in $[Ni_6(\eta^5\text{-}C_5H_5)_6][PF_6]$, which has a perfect NaCl structure. It is significant that the P_{c-a} value for this salt is zero since this implies that the ionic spheres defined by R_{eff} for this salt are in contact but are not interpenetrating, *i.e.* that R_{eff} is a very good estimate of molecular or ionic size.

The factors which are going to prevent a salt from adopting a structure based on size considerations alone are (*i*) large deviations from sphericality of either the anion or cation, (*ii*) a large degree of interpenetration between neighbouring ions, and (*iii*) strong directional Coulombic or van der Waals interactions. All three effects have been observed in the eleven hexafluorophosphate salts studied.

The first effect is most clearly visible in Fig. 5(*a*), where the six nearest-neighbour anions around the $[Fe(CO)_3(\eta^5\text{-}C_6Me_7)]^+$ cation have split into a set of four close ones and two at a further distance, consistent with the discoidal shape of the cation. This effect is present in all the structures studied, but for most of them the effect is small since their ions do not deviate too greatly from the spherical ideal. The ellipsoid representation of ions developed in this paper provide an effective methodology for describing these shape effects.

The presence of interpenetration of neighbouring ions in the hexafluorophosphate salts is indicated by the interpenetration indices listed in Table 4. All the P_{a-a} indices are positive, indicating that no interpenetration between hexafluorophosphate anions is occurring. This is not surprising since this anion is smaller than all the cations studied, preventing the anions from being in contact. The P_{c-c} indices are much more interesting, with generally larger values as the cation size increases. This is because as the ion gets larger, the cation–cation van der Waals interactions become the dominant factor in the lattice energy at the expense of the Coulombic interactions. As a result, the large cations try to fit together as tightly as possible, leaving the anions to occupy the cavities left in the lattice. This tendency can be observed in the ellipsoid diagrams presented in this paper. For the smaller cations, the distribution of the anions around the cations has been shown to be dependent on the shape of the cation. For the larger ions this is not the case, but examination of the arrangement of cations around an anion shows that the cations are arranged to pack most efficiently with each other.

It is also cation–cation interpenetration that is allowing four-co-ordination to take place with a larger a/c ratio than that suggested by the spherical ideal. The interpenetration between cations within a layer generates gaps above and below the anions that are too small to accommodate another cation, thus preventing octahedral co-ordination. This also explains why no four-co-ordinate structures with tetrahedral co-ordination are observed, since to achieve this, a spherical cation larger than $[Au(PPh_2Me)_4]^+$ with a large R_{eff}/R_{max} ratio of more than 0.75 to prevent interpenetration, is required. The cation–anion interpenetration values for the hexafluorophosphate salts are less important. The two largest values reported in Table 4 are spurious, since the cations in these two salts are those which are least spherical. The P_{c-a} index is expected to be important in the tetraphenylborate salts which will be discussed in the next paper in this series.

The presence of strong dipolar and van der Waals interactions have been determined by calculating the lattice energies of the hexafluorophosphate salts. These calculations have included a Coulombic term, calculated using both unit charges and partial atomic charges. These calculations have shown that both the van der Waals and Coulombic energies are roughly linear with respect to the effective radius of the cation. The van der Waals energy became more negative as the effective radius was increased whilst the Coulombic energy became less negative, leading to a fairly constant value of about -550 kJ mol^{-1} for the lattice energy. Several salts were found to have van der Waals energies less than that predicted from the size of the cation. These salts were found to have higher Coulombic energies than expected, which compensated for the loss in van der Waals energy. This effect was most prominent in the unusual five-co-ordinate packing motif found for $[Ru(N_3)(N_2)(en)_2][PF_6]$, where the inefficient packing of the ions was stabilised by interactions between the highly polarised azide groups on neighbouring cations.

Acknowledgements

A. L. R. thanks the British Council and the Association of Commonwealth Universities for his Commonwealth Scholarship. Thanks are also due to the Air Force Office of Scientific Research for financial support of this project. We also acknowledge the extensive use of the CHEM-X modelling system, Chemical Design Ltd, Oxford throughout this project. All the packing diagrams and ion environment diagrams presented in this work were generated by the MolDraw software.[35]

References

1 G. R. Desiraju, *Crystal Engineering: The Design of Organic Solids*, Elsevier, Materials Science Monographs, 1989, vol. 54.
2 J. M. Williams, H. H. Wang, T. J. Emge, U. Geiser, M. A. Beno, P. C. W. Leung, K. D. Carlson, R. J. Thorn, A. J. Schultz and M. H. Whangbo, *Prog. Inorg. Chem.*, 1987, **35**, 218.
3 J. S. Miller, A. J. Epstein and W. M. Reiff, *Acc. Chem. Res.*, 1988, **21**, 114.
4 W. Tam and J. C. Calabrese, *Chem. Phys. Lett.*, 1988, **144**, 79.
5 M. L. H. Green, S. R. Marder, M. E. Thompson, J. A. Bandy, D. Bloor, P. V. Kolinsky and R. J. Jones, *Nature (London)*, 1987, **330**, 360.
6 D. L. Cocke and A. Clearfield, *Design of New Materials*, Plenum, New York, 1987.
7 D. Braga, F. Grepioni and P. Sabatino, *J. Chem. Soc., Dalton Trans.*, 1990, 3137.
8 U. Müller, *Acta Crystallogr., Sect. B*, 1980, **36**, 1075.
9 D. Braga and F. Grepioni, *Organometallics*, 1992, **11**, 1256.
10 F. H. Allen, S. A. Bellard, M. D. Brice, B. A. Cartwright, A. Doubleday, H. Higgs, T. Hummelink, B. G. Hummelink-Peters, O. Kennard, W. D. S. Motherwell, J. R. Rodgers and D. G. Watson, *Acta Crystallogr., Sect. B*, 1979, **35**, 2331.
11 D. M. P. Mingos and A. L. Rohl, *J. Chem. Soc., Dalton Trans.*, 1991, 3419.
12 A. Gavezzotti, *J. Am. Chem. Soc.*, 1983, **105**, 5220.
13 V. Schomaker, J. Waser, R. E. Marsh and G. Bergman, *Acta Crystallogr.*, 1959, **12**, 600.
14 SNOOPI—part of the CRYSTALS package by D. J. Watkin and P. W. Betteridge, Chemical Crystallography Laboratory, University of Oxford.
15 H. Lipson and W. Cochran, *The Determination of Crystal Structures*, G. Bell and Sons Ltd, London, 1966, vol. 3.
16 D. E. Williams and D. J. Houpt, *Acta Crystallogr., Sect. B*, 1986, **42**, 286.
17 E. Giglio, *Z. Kristallogr.*, 1970, **131**, 385.

18 R. Hoffmann and W. N. Lipscomb, *J. Chem. Phys.*, 1962, **36**, 2179.
19 D. E. Williams, *Acta Crystallogr., Sect. A*, 1972, **28**, 629.
20 Y. Wang, L. D. Calvert and S. K. Brownstein, *Acta Crystallogr., Sect. B*, 1980, **36**, 1523.
21 M. E. Gress and R. A. Jacobson, *Inorg. Chem.*, 1973, **12**, 1746.
22 B. R. Davis and J. A. Ibers, *Inorg. Chem.*, 1970, **9**, 2768.
23 Y. V. Gatilov, N. G. Bokii and Y. T. Struchkov, *Zh Strukt. Khim.*, 1975, **16**, 855.
24 P. M. Treichel, J. W. Johnson and J. C. Calabrese, *J. Organomet. Chem.*, 1975, **88**, 215.
25 M. R. Thompson, C. S. Day, V. W. Day, R. I. Mink and E. L. Muetterties, *J. Am. Chem. Soc.*, 1980, **102**, 2979.
26 I. H. Williams, D. Spangler, D. A. Femec, G. M. Maggiora and R. L. Schowen, *J. Am. Chem. Soc.*, 1980, **102**, 6621.
27 T. V. Ashworth, A. A. Chalmers, D. C. Liles, E. Meintjies, H. E. Oosthuizen and E. Singleton, *J. Organomet. Chem.*, 1985, **284**, C19.
28 B. E. Reichert, *Acta Crystallogr., Sect. B*, 1976, **32**, 1934.
29 G. J. Kruger and R. O. Heckroodt, *J. Organomet. Chem.*, 1976, **111**, 225.
30 R. C. Elder, E. H. K. Zeiher, M. Onady and R. R. Whittle, *J. Chem. Soc., Chem. Commun.*, 1981, 900.
31 J. D. McCullough, *Acta Crystallogr.*, 1964, **17**, 1067.
32 A. F. Wells, *Structural Inorganic Chemistry*, Oxford University Press, Oxford, 5th edn., 1984.
33 P. Boher, P. Garnier, J. R. Gavarri and A. W. Hewat, *J. Solid State Chem.*, 1985, **57**, 343.
34 A. Gavezzotti, *J. Am. Chem. Soc.*, 1989, **111**, 1835.
35 J. M. Cense, *Tetrahedron Comput. Method.*, 1989, **2**, 65.

Received 16*th June* 1992; *Paper* 2/03128K